

Interaction Notes

Note 612

25 October 2009

INDUCED TRANSIENTS ON AN UNDERGROUND CABLE BY HYPERBAND SIGNALS

K. Sunitha

Pulsed Power and EMC Laboratory

Department of Electrical Engineering

Indian Institute of Science, Bengaluru- 560012, INDIA

Prof. M. Joy Thomas

Pulsed Power and EMC Laboratory

Department of Electrical Engineering

Indian Institute of Science, Bengaluru-560012, INDIA

Dr. D.V.Giri

Pro-Tech, 11-C Orchard Court, Alamo, CA 95407-1541 USA

Department of Electrical and Computer Engineering, University of New Mexico,

Albuquerque, NM. USA

Abstract

The reflector type of impulse radiating antenna (IRA) has been used for a wide variety of applications in both military and civilian domains. This paper deals with the interference caused on underground cables due to electromagnetic fields from IRA's. The induced current and voltage on a cable when it gets illuminated by an IRA is determined. This computation is preceded by the computation of radiated electromagnetic fields from an IRA both in the near field and in the far field regions.

1. Introduction

Impulse radiating antennae have wide variety of applications such as the detection of buried objects, ionospheric research and target discrimination in a cluttered environment [1, 2]. The hyperband electromagnetic fields [3] coming out of the IRAs can interfere with the objects in the path where it travels. This can be an object laid underground or any object on or above the ground.

Underground cables are used to a greater extent now-a-days for communication purposes in urban cities and towns. Some of the frequencies of the electromagnetic fields from an IRA can easily penetrate through the soil and can reach the buried cable. This will illuminate the cable with the UWB fields and induce currents and voltages in it. Since the communication cables or even the buried data cables are connected to sensitive equipment, even a slight rise in the voltage or the current at the terminals of the equipments can become a serious problem for the smooth operation of the system. In this aspect it is worthwhile to determine the effect of an IRA's electromagnetic field on the cables laid underground. Treating this as an electromagnetic compatibility problem, the victim circuit becomes the cable, the source of interference being the electric field from the IRA and the air and soil forms the path of propagation of the interference signal to the victim circuit. As a first step to this computation, we need to know the exact nature of the electromagnetic field from an IRA at different distances from the antenna. Using the concept of the reflection and transmission of the field at the earth's surface, the amount of the field coupling to the cable can be found. This in turn can be used for the determination of the induced current and voltage on the cable which give an exact measure of the interference on the cable. This work deals with the coupling effect of IRA fields on buried telephone cables.

2. Impulse Radiating Antenna

A parabolic reflector type IRA [4] has been considered as the source of interference which is shown in figure 1. The reflector is fed by a transverse

electromagnetic wave structure energized by a $\pm 60kV$ source. The detailed description of the source is available in [2, 4]. The characteristic properties of this antenna includes the far field electric field measured in the boresight at $r = 305m$ being equal to $4.2kV/m$, the uncorrected pulse rise time (10%-90%) equal to 99ps and the boresight electric field's FWHM equal to 130ps. The pulser output voltage is different from the voltage launched on the antenna on account of the presence of other dielectric media at the feed point [5].

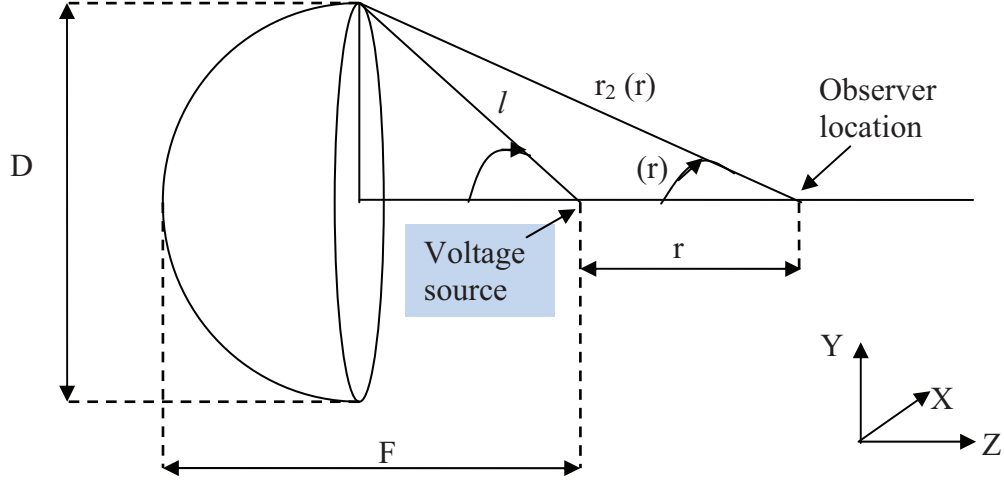


Figure 1. A parabolic reflector type IRA

Instead of the normally used double exponential model, an analytical model has been used to describe the output voltage, according to which the pulser output voltage, its derivative and the Fourier Transform can be written as [2, 4]

$$V(t) = \begin{cases} V_0 e^{-(\beta(t/t_d))} \left(\frac{1}{2} \operatorname{erfc} \left(\sqrt{\pi} \frac{|t|}{t_d} \right) \right) & t < 0 \\ V_0 e^{-(\beta(t/t_d))} \left(1 - \frac{1}{2} \operatorname{erfc} \left(\sqrt{\pi} \frac{|t|}{t_d} \right) \right) & t > 0 \end{cases} \quad (1)$$

$$\frac{dV(t)}{dt} = \frac{V_0}{t_d} e^{-(\beta(t/t_d))} e^{-\pi(t/t_d)^2} - \frac{\beta}{t_d} V(t) \quad (2)$$

$$\tilde{V}(\omega) = \frac{V_0 t_d}{(\beta + j\omega t_d)} e^{\left\{ \left(\frac{1}{4\pi} \right) (\beta + j\omega t_d)^2 \right\}} \quad (3)$$

For the pulser feeding the IRA, these parameters are [2, 4]

$$V_0 = 120.72 \text{kV} \quad t_d = 100 \text{ps} \quad = 0.005 \\ (\text{d}V/\text{dt})_{\text{max}} = 1.2 \times 10^{15} \text{ V/s.} \quad (4)$$

The peak amplitude of the voltage waveform is slightly less than V_0 . We find that with V_0 of 120.72 kV, the peak amplitude turns out to be 120 kV. The details of the pulser and the antenna assembly are described in detail in [6]. The above outlined model is depicted in the figure 2 for the voltage. This voltage is used for the computation of the electric field and hence for the determination of the induced current and voltage on the cable.

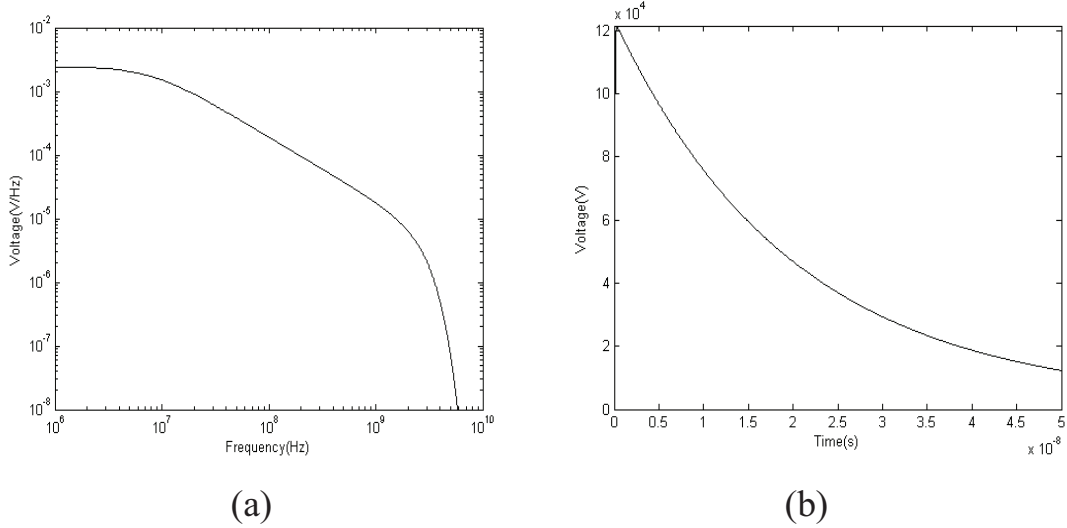


Figure.2 Output voltage of the pulser (a) Frequency domain (b) time domain

2.1. Electric fields from IRA

The electric field from IRA at any observation point can be found out by integrating over the aperture the equivalent magnetic currents (\vec{M}) given by [7]:

$$\vec{M} = 2\hat{z} \times \vec{E}_{\text{aperture}} \quad (5)$$

Where $\vec{E}_{aperture}$ is the numerically computed electric field at the aperture of the IRA with an FDTD code. Using this, the x, y and z components of the electric fields at any point can be obtained from the following well known equations

$$E_x = -\frac{1}{4\pi} \iint_{aperture} (z-z') M_y \frac{1+jkR}{R^3} e^{-jkR} dx' dy' \quad (6)$$

$$E_y = \frac{1}{4\pi} \iint_{aperture} (z-z') M_x \frac{1+jkR}{R^3} e^{-jkR} dx' dy' \quad (7)$$

$$E_z = -\frac{1}{4\pi} \iint_{aperture} [(y-y') M_x - (x-x') M_y] \frac{1+jkR}{R^3} e^{-jkR} dx' dy' \quad (8)$$

where (3) and (4) are used as inputs to these equations.

2.2. Electric field along the boresight from IRA

The electric field can be computed at any given point along the boresight by taking only its z component as given by expression (7) and is plotted in figure 3 at distances 5m, 10m, 20m, 100m and 304m from the IRA. This figure gives the frequency domain representation of the electric field (computed by using the aperture integrals) at all the above observation points which cover the whole range from the near field through the intermediate field and to the far field.

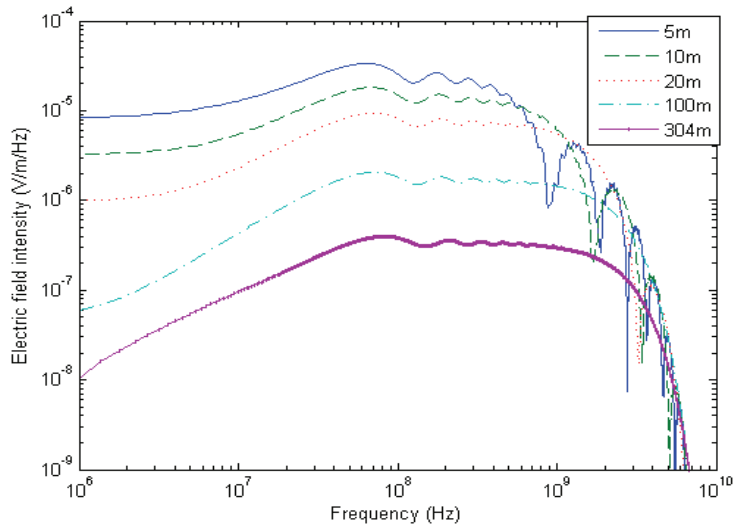


Figure 3. Electric field at different points along the boresight in frequency domain

This figure shows that the spectrum becomes oscillatory at higher frequencies in the near field but in the intermediate and the far fields the fields have less oscillation. Figure 4 represents the time characteristics of the fields at the same points ie. 5m, 10m, 20m, 100m and 304m. We can see that whatever be the distance, the electric field has a negative portion (prepulse) up to 8ns ($= 2 F/c$) with F and c being the focal length of the reflector and speed of light in air respectively), followed by its impulsive transient nature. This 8ns accounts for the time taken by the pulse to travel to the reflector's surface and get itself felt at the source point. Till then there is a direct radiation of the feed pulse at the observation point, which is negative in nature on account of its reverse travel. This 8ns time is common for all the observation points with far fields getting a lesser magnitude of the pulse and near field getting a large negative portion. Since the area under the negative and the positive portions of the wave has to be equal it is reflected in the relative magnitudes of the positive and the negative signals. Hence the magnitude of the signal shoots to a maximum at around 20m where the observation point is in the near field. Here the peak negative value of the field intensity is 996V/m and the positive value of the field intensity is 27kV/m. At 5m the respective figures are 3600V/m and 25kV/m. In the intermediate field i.e., at 100m these figures come to 284.5V/m and 13kV/m respectively and in the far field i.e., at 304m, these are 90V/m and 4951V/m respectively.

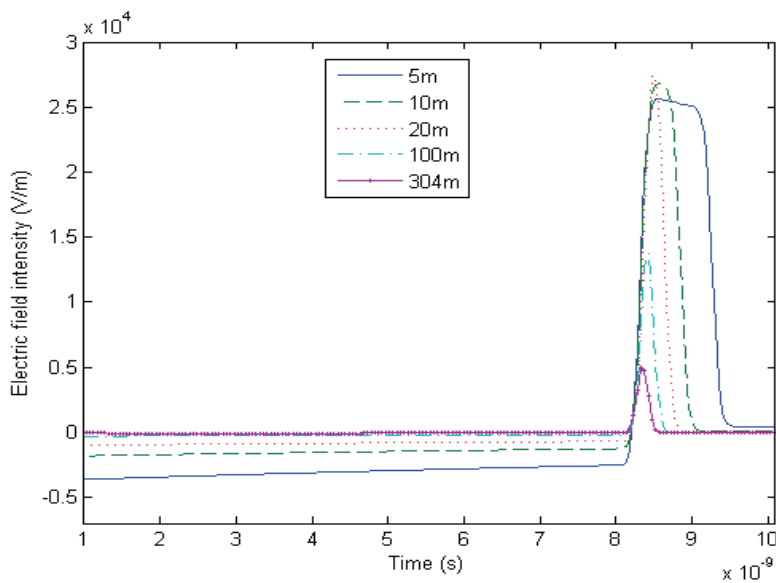


Figure 4. Electric field at different points along the boresight in time domain

2.3. Electric field perpendicular to the boresight from IRA

The expressions (5), (6), (7) together can give the electric field at any given observation point. This analysis is required for the next section where we want to analyze the fields at different points along the cable that is finally going to excite our cable structure. Hence the fields along distances perpendicular to the boresight is computed in this section. This analysis is done for two observation points one in the near field at 5m and the other in the far field at 304m. These computed results are plotted in figures 5 to 8. In these computations, the boresight of the IRA meets the x axis at an arbitrary distance of 5m away from the reference point $x=0\text{m}$. From figures 5 and 6, it can be seen that $x=0\text{m}$ and $x=10\text{m}$ locations are both at equal distances from the boresight and hence the graphs are overlapped. Furthermore, in the near field, up to 30m perpendicular to the boresight in either direction, significant high frequency radiation is present. Whereas in the far field, this is only up to 15m on either side. This is indicative of the directivity of the radiation in the far field. A mesh plot showing the combined variation of the distance perpendicular to the boresight and the time response is obtained from figures 7 and 8. These two graphs show that the graph becomes peakier in the far field and it is broader in the near field.

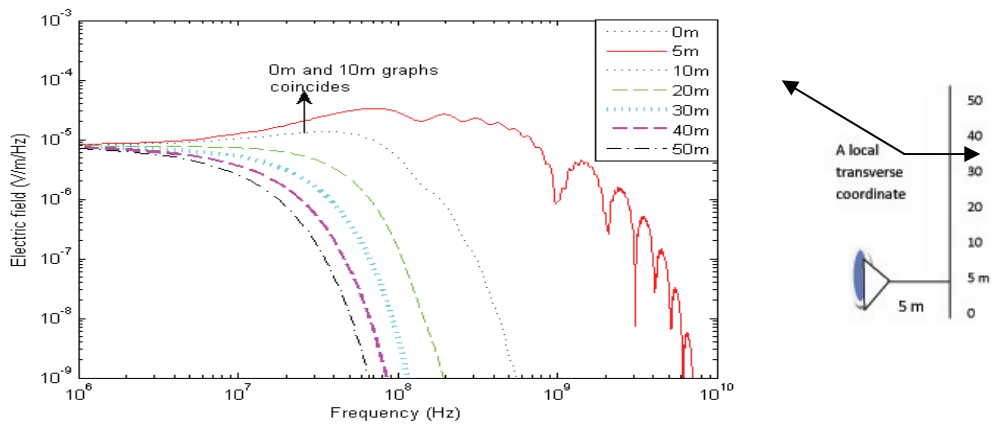


Figure 5. Electric field at 5m in air at points perpendicular to the boresight in frequency domain. (The 0m and 10m graphs coincide.)

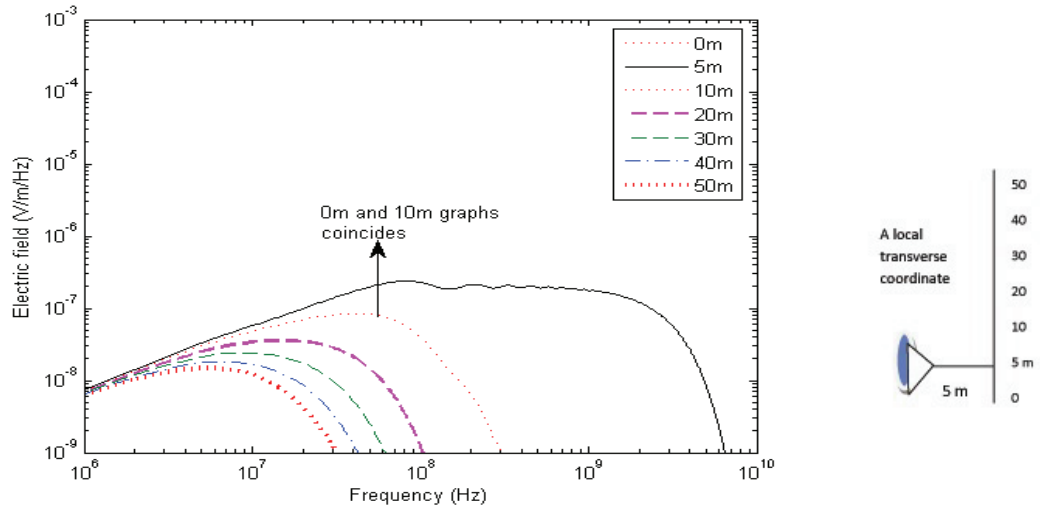


Figure 6. Electric field at 304m in air at points perpendicular to the boresight in frequency domain (The 0m and 10m graphs coincide.)

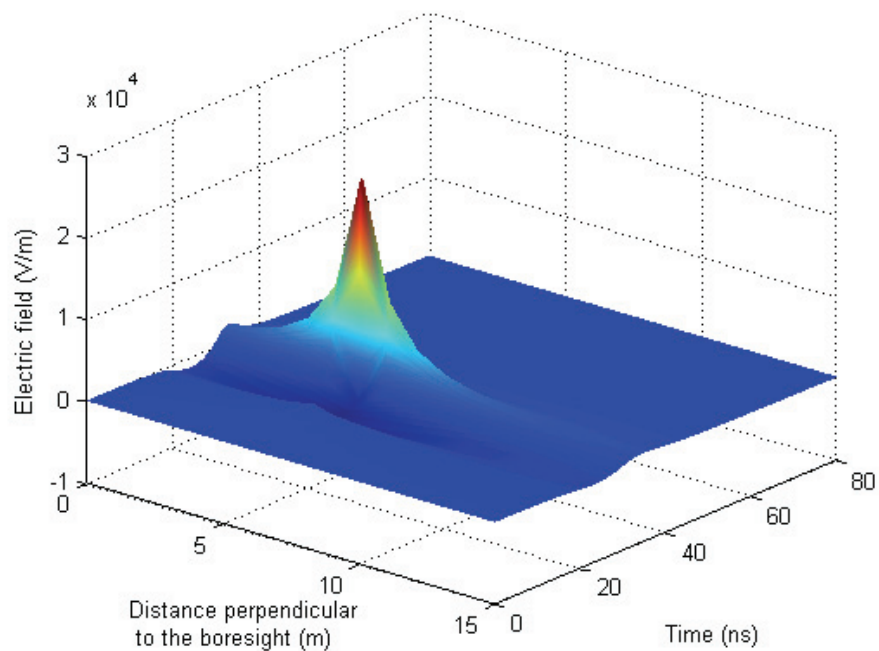


Figure 7. Electric field at 5m in air at points perpendicular to the boresight in time domain

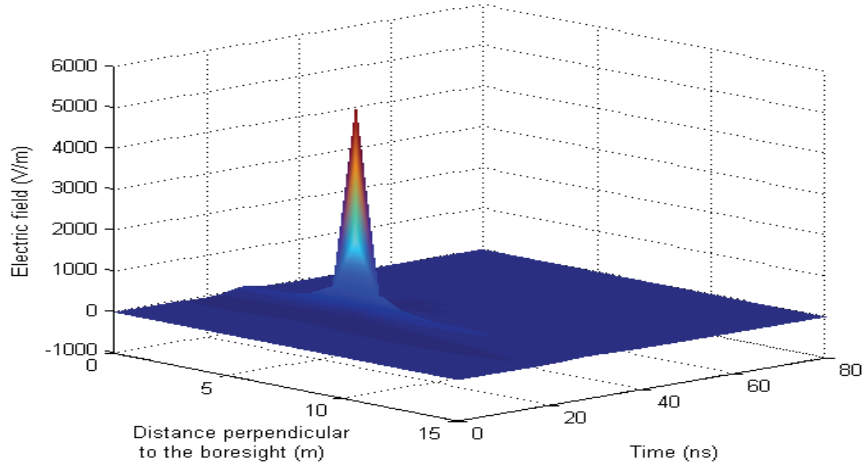
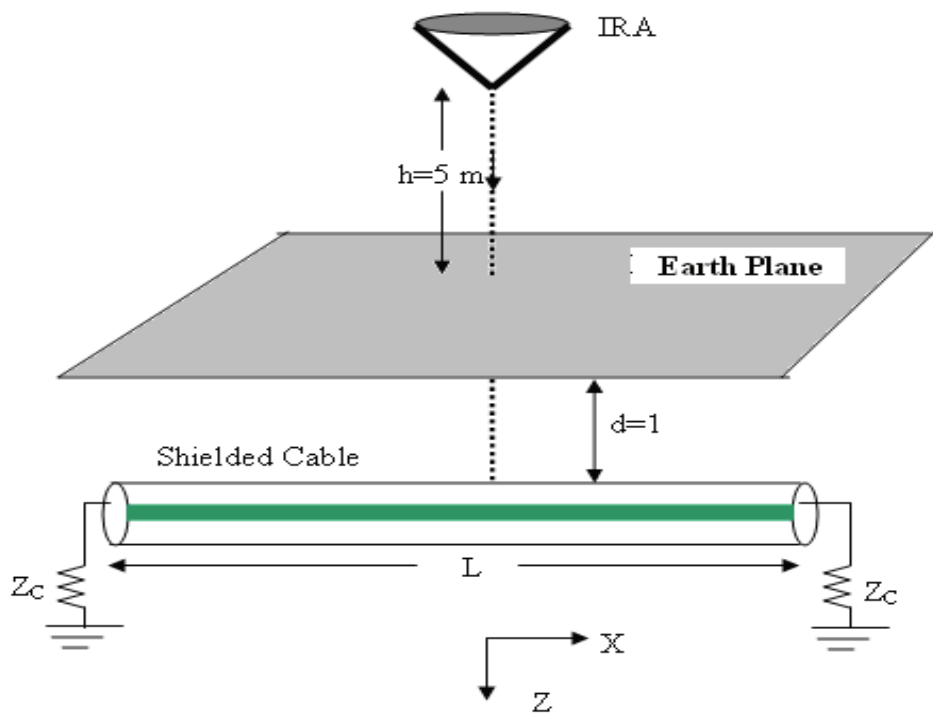


Figure 8. Electric field at 304m in air at points perpendicular to the boresight in time domain

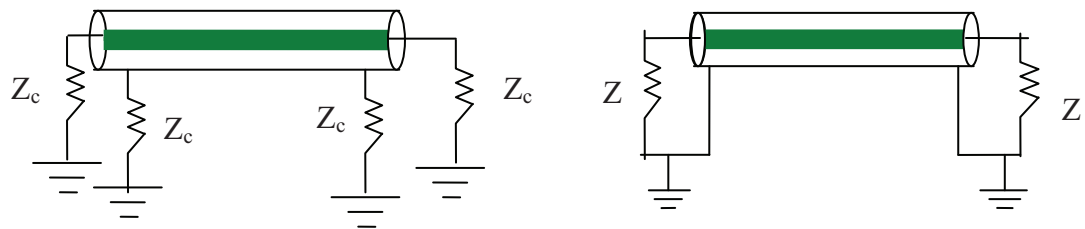
3. IRA illuminating the cable

This section considers the effect of an underground cable getting illuminated by an IRA. This situation is portrayed in figure 9. Figure 9A shows the antenna and the buried cable geometry, while figure 9 B shows the details of termination.

The IRA is located at a height of 5m above the ground. The cable is buried at a depth of 1m below the ground and is excited by the electric field generated by the IRA. The earth plane is considered to be of infinite extent. The cable is buried such that the boresight of the IRA meets the cable at a distance of 5m from its one end. In this work only direct radiation by IRA is considered. The cable is terminated at both ends by matching impedances. The conductivity of the soil is taken as 0.001S/m. The relative dielectric constant of the soil is assumed to be 10. The cable is a shielded cable used for the communication purposes. The cable consists of a large number of fine conductors, each of very small diameters, close to each other in a given small volume of the cable inner core, the number of cores dependent on the application. The skin effect and proximity effect can be neglected at the incident large field amplitude, as the cable is in the near field.



A. Impulse radiating antenna illuminating a buried cable



B. Details of the two possible termination schemes of the shielded cable

Figure 9. IRA and the buried cable geometry along with termination details

Both the shield and the inner conductor are terminated respectively by their own characteristic impedances to earth. This means that the inner conductor has Z_{ci} to earth and shield also has Z_{cs} to earth. We have also tried out the second case when the inner conductor is terminated to the shield and then grounded which makes a difference in the induced parameters. It is clear that the nature of the termination is critical in the evaluation of the induced parameters. In our case of figure 9B (left side termination), there are no reflections of the shield current at the ends and likewise there is no reflection of the current in the inner conductor at the ends of the cable.

So we can simulate the cable as a coaxial one. The cross section of the cable is shown in figure 10. The dimensions of the cable are also shown in the same figure. The outer insulation and the inner insulation used is PVC. The conductor is made of copper. The shielding is done using galvanized steel. The cable length used in the study is 10m.

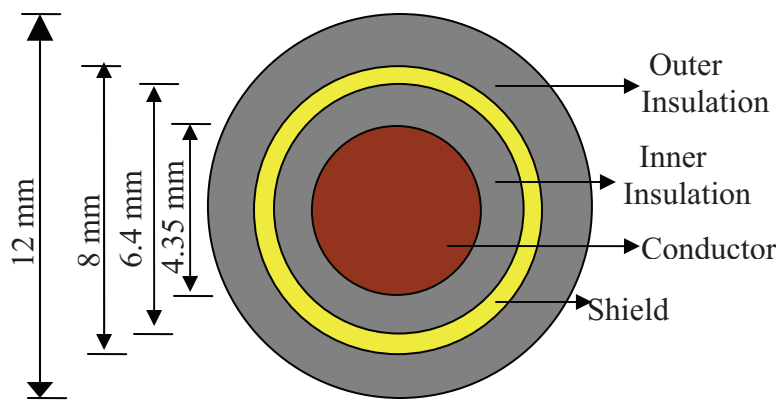


Figure 10. Cross section of the cable

3.1. Electric field at the cable location

Using (5), (6) and (7) the electric fields have been computed at a distance of 5m in air. Fresnel's reflection and transmission coefficients can be used to compute the percentage of the field illuminating the cable. These computed results are plotted in figure 11 and figure12. Figure 11 shows the electric fields at different points along the

length of the cable in frequency domain. $x=0\text{m}$ corresponds to one end of the cable and $x=10\text{m}$ corresponds to the other end. This figure shows that for the configuration of the system considered, the entire cable gets illuminated by the UWB pulses having frequency component up to 1GHz and for frequencies above this, only the boresight is getting illuminated. ***So the problem of coupling to the cable is a case of frequency dependent distributed excitation.*** The time nature of the field as a function of the distance along the cable length is shown in figure 12. The peak value of the field comes to 12kV/m at 5m where the boresight touches the cable. The field falls off gradually on either side with distance along the cable length. It is also clear from figure 12, that it takes about 80 ns, after the IRA voltage is turned on for the electric field along the entire length of the cable to be established to the fullest. The induction of current on the shield is then expected to start at this time $t = t' = 80$ ns.

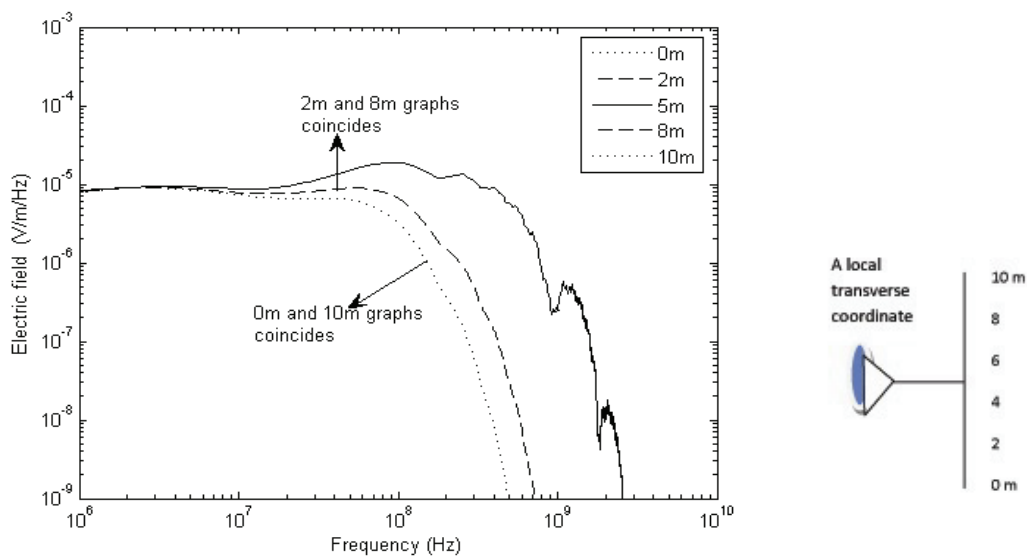


Figure 11. Frequency domain representation of the electric field along the length of the cable

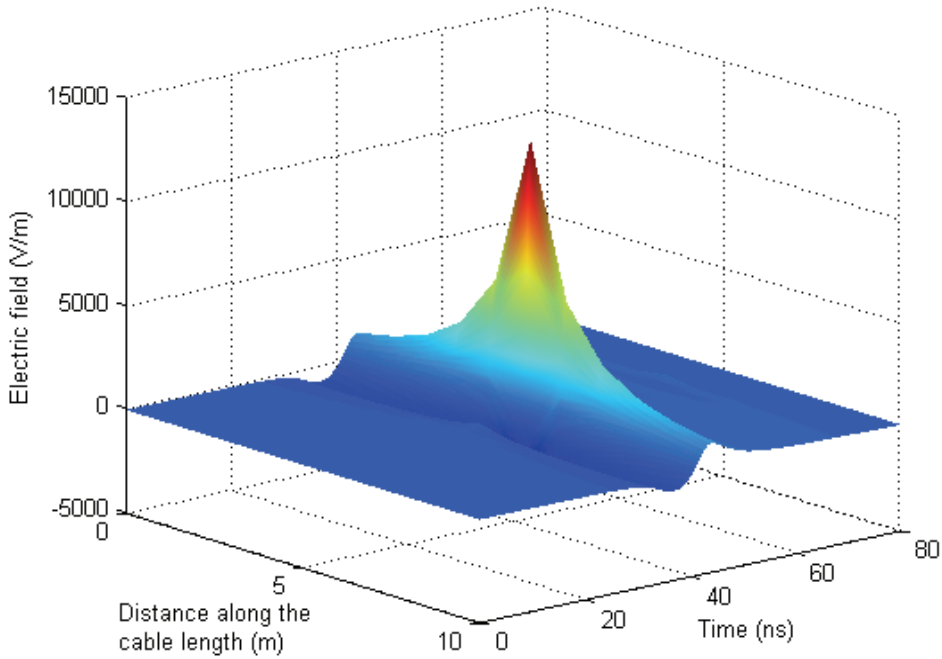


Figure 12. Time domain representation of the electric field along the length of the cable

4. Coupling to the cable

Coupling with the cable can be considered in two stages: coupling to the external circuit and coupling to the internal circuit. The detailed circuit configuration of the two circuits is given in figure 13. The external circuit consists of the soil whose impedance is taken as Z_g and admittance Y_g , the outer layer of shield whose impedance is taken as Z_{sh} and the outer dielectric layer which has a series impedance of Z_{ins} and a capacitance of X_c ; the inner circuit consists of the inner insulation of impedance Z_{ind} and admittance Y_{ins} , conductor of impedance Z_{wire} and the inner layer of the shield of impedance Z_{ss} . The two circuits are coupled by means of the shield transfer impedance, Z_t . The value of the transfer impedance is frequency dependant and is a function of the shield thickness. The value of Z_t is computed using Schelkunoff's equation [8].

The incident UWB electric field reaching the cable will induce current in the shield. This can be determined by assuming the shield as a single core conductor with an outer layer of insulation. At all the points along the length of the shield there is an

excitation due to the field. This is a case of the distributed excitation and hence current is induced at every point on the cable at the same time. These currents propagate to both the ends where it suffers reflections from the terminations. The method of analysis should accommodate for these effects. Transmission line analysis was found to be suitable for such a case and hence is adopted in this work. This analysis uses the governing equations for the induced current and voltage as given in the following equations, [9]

$$\frac{dV_e(x)}{dx} + (Z)I_e(x) = E(x, z=d) \quad (8)$$

$$\frac{dI_e(x)}{dx} + YV_e(x) = 0 \quad (9)$$

$$I_e(x) = \int_0^L G_I(x, x_s) E(x_s, z=d) dx_s \quad (10)$$

$$V_e(x) = \int_0^L G_V(x, x_s) E(x_s, z=d) dx_s \quad (11)$$

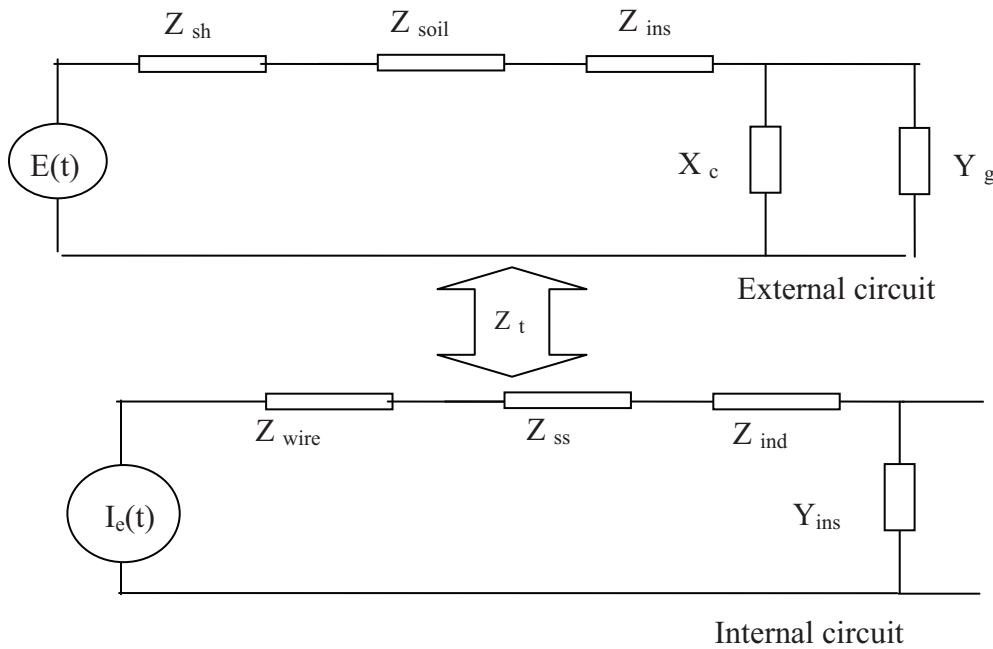


Figure 13. Circuit representation of the cable

The transfer impedance that couples the shield current to the interior signals is shown plotted in figure 14. Reference [10] discusses a similar cable and provides equations to estimate the transfer impedance, which have been used here. The characteristic impedance in our case is qualitatively similar to the cable considered in [10].

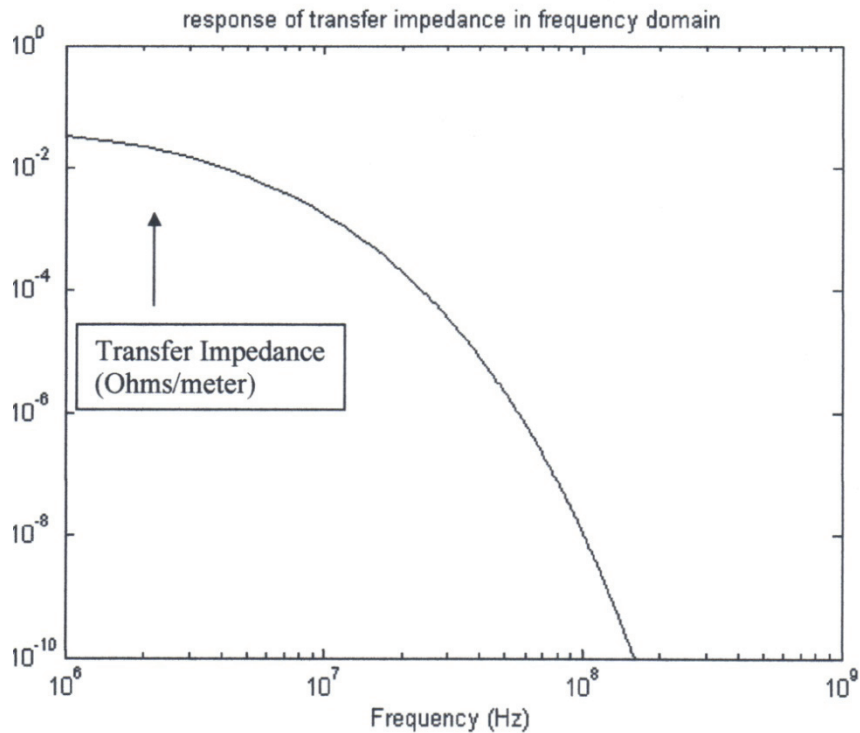


Figure 14. Transfer impedance as a function of frequency

The value of transfer impedance varies with frequency as shown above. The transfer impedance is tens of milli-ohms per meter at low frequency. In this work a copper tubular shield is considered with no braiding. For such cables the transfer impedance drops with frequency. Another example of such a cable can be seen in [10].

In these equations, $V_e(x)$ and $I_e(x)$ are the induced voltage and current at any point on the shield. $E(x, z=d)$ is the transmitted component of the incident UWB field which illuminates the cable. Z is the net series impedance of the external circuit and Y is its admittance. Since this is the case of a distributed excitation, the current at any point on the shield should be the sum of the incident and the reflected (from cable terminations) components of the current. This addition is taken into account in (10) where G_I is the

Green's function which automatically takes care of this addition. When current is induced in the shield, not all of this current gets coupled to the inner circuit. Only a small portion of this shield current gets coupled to the inner circuit, which is given as $Z_t^* I_e(x)$ where Z_t ohms is the transfer impedance of the shield. The induced current in the inner conductors can be determined from the following equation [9].

$$\frac{dV_i(x)}{dx} + (Z_i)I_i(x) = Z_t I_e(x)$$

(12)

$$\frac{dI_i(x)}{dx} + Y_i V_i(x) = -Y_t V_e(x) \quad (13)$$

Where $V_i(x)$ is the induced voltage at any point x in the inner conductor and $I_i(x)$ is the induced current at that point. Z_i is the impedance of the inner series circuit. Y_i is the admittance of the inner circuit [12], [11]. Y_t is the transfer admittance which is very small so that it can be neglected. The induced voltage on the inner conductor at any point x in the cable can be computed using Green's functions [11] as:

$$I_i(x) = \int_0^L G_i(x, x_s) Z_t I_e(x_s) dx_s \quad (14)$$

$$V_i(x) = \int_0^L G_v(x, x_s) Z_t I_e(x_s) dx_s \quad (15)$$

The Green's functions are not explicitly written here and can be found in [9 and 11].

4.1 Induced current in the cable

For the cable configuration shown in figure 10, the induced current is computed using (10) and (14) and the result is depicted in figure 15 for the shield at different points. The peak current in the cable is 10A at 5m along the cable length where the boresight exactly meets the cable. This is due to the prolonged radiation at that point. This is

expected because of the initial direct radiation at the observation point which can be seen in the electric field plot in figure 4. At $x=0m$, $x=2m$ and $x=10m$, the currents at other points are smaller. The currents at $x = 0m$ and $x = 10m$ are also seen to be identical as they are symmetric points with respect to the antenna. The nature of the current as a function of the distance along the length of the cable and the time is given in figure 16. This figure indicates that the current initially peaks at 5m and slowly as time progresses the other points also gets the signal and hence the peak shifts sideways. This is due to the traveling wave components of the UWB pulses that start at the point where the boresight is located, which is at 5m away from one end of the cable, and slowly moves to the ends with a finite velocity. As there are no reflected components of the current traveling wave, the peak in the waveform shows a shift with time which is a function of the velocity of propagation in the soil that in turn depends on the soil characteristics. The time reference or $t = 0$ is when the IRA voltage is turned on and it takes certain time interval for the induced quantities to start appearing. This is clearly seen in figure 15. The time taken for the antenna to establish electric field fully on the cable from figure 12 is 80 ns. The voltage of the shield with respect to the reference conductor is established at $t = 80\text{ns}$. The currents now can begin to flow.

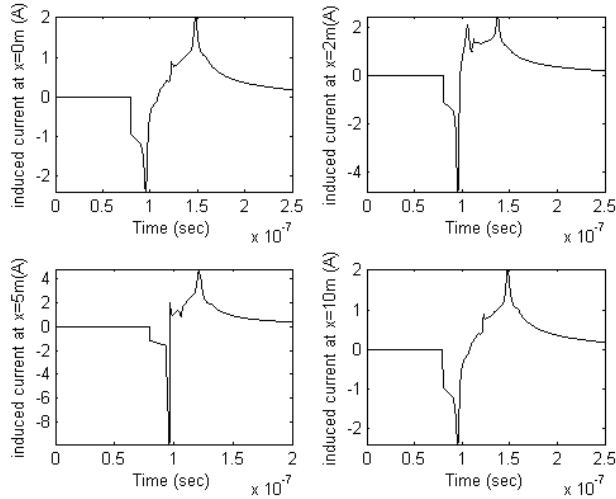


Figure 15. Induced current in the shield at different points

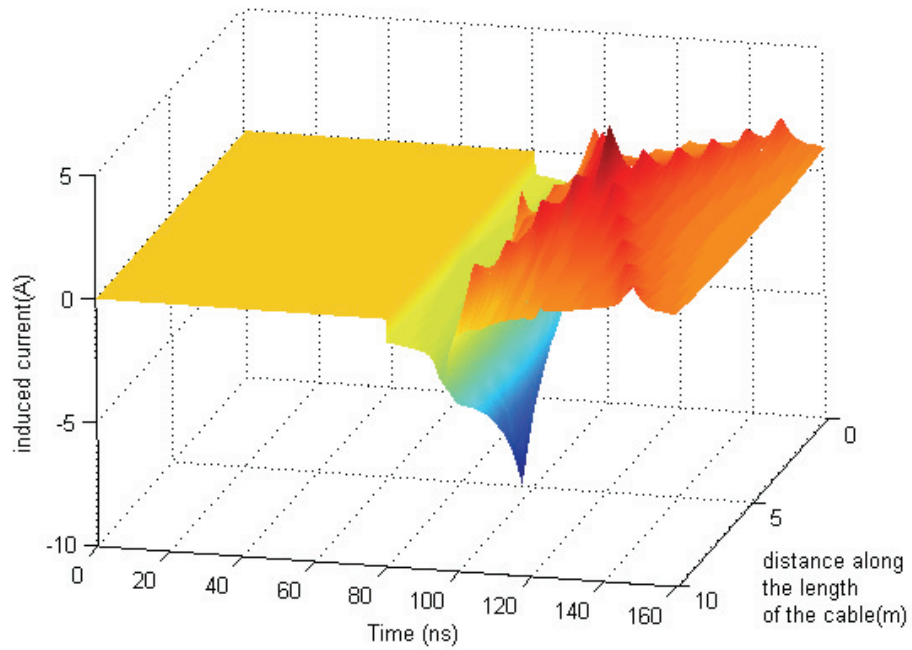


Figure 16. Induced current in the shield as a 3-dimensional plot

The prepulse which is followed by the impulse, is the character of the illuminating field and this is also seen in the currents. The duration of the prepulse in air is $2 F/c = 8\text{ns}$. However the prepulse has to travel an extra meter in soil and hence $\{(2F/c) + (1\text{meter}/v \text{in soil})\}$ turns out to be 18.6 ns , with speed of light in soil $\sim 9.4 \times 10^7 \text{ m/s}$. Hence the prepulse nature of the currents last for 18.6 ns as seen in the current plots. There are no resonances in the current, since the terminations are such that there are no reflections permitted at the end. Of course this statement is approximate in the sense the characteristic impedance is a function of frequency and, in practice, there will be some reflections at the terminations. The current in the shield of the cable acts as a secondary source of excitation to the inner conductor and hence causes the induced current in the cable which is computed and plotted in figure 17 and figure 18. The inner conductor currents start after quite some time (in this case $\sim 400\text{ ns}$) after the IRA voltage is turned on. It is seen that current magnitude is same everywhere with the current having a

magnitude of -1.7mA. The current is negative as its path is in the opposite direction when compared to the current induced in the shield of the cable. Figure18 shows the mesh plot of the induced current as a function of the cable length and time. It can be seen that all parts of the inner conductor are simultaneously prone to UWB interference.

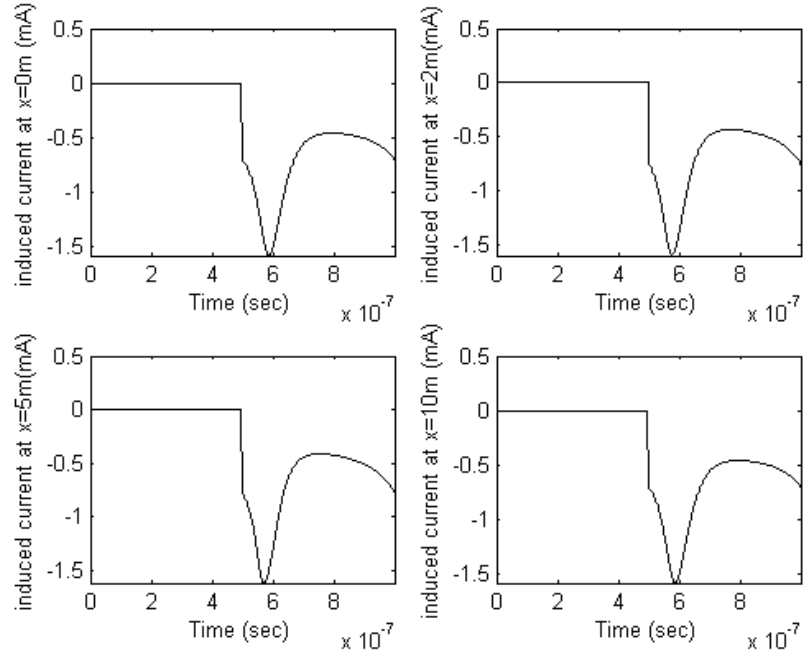


Figure 17. Induced current in the inner conductor at different points

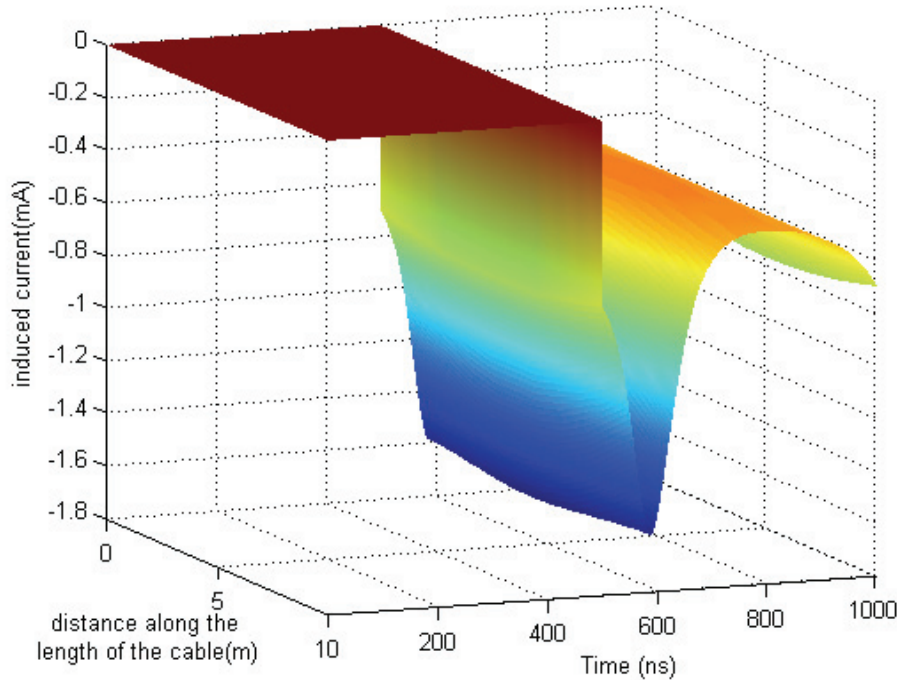


Figure 18. Induced current in the inner conductor at different points

4.2 Induced voltage on the cable

Induced voltage is a representative of the electrostatic coupling to the cable on account of the capacitance in several sections of the cable. The induced voltage is computed using (11) and (15) and is shown in figure 19 and figure 20 for the shield and in figure 21 and figure 22 for the inner conductor. The voltage in figure 20 appears to be somewhat spiky, perhaps due to insufficient sampling along the cable. It is likely that the accuracy can be improved by a finer sampling. The voltage in the shield reaches a maximum value of 350V at a distance of 5m off the end point where the boresight meets the cable; the nature of the voltage at that point is identical with the electric field at the cable location at 5m. All other points like 0m, 2m, and 10m the peak magnitude of the voltage are given by -250V, -220V and 250V respectively. For distances along the cable from $x=0$ m up to the boresight, there is a negative traveling wave of voltage and hence the peak voltage is negative and the points from $x=5$ to $x=10$ m have a positive traveling wave of voltage and hence has positive magnitude of the peak voltage. The similarity in

the parameters for 0m and 10m is due to their identical locations along the cable off the boresight. Furthermore, the oscillations seems to increase from the boresight to the off boresight points because of the impact of the soil characteristics and the cable parameters.

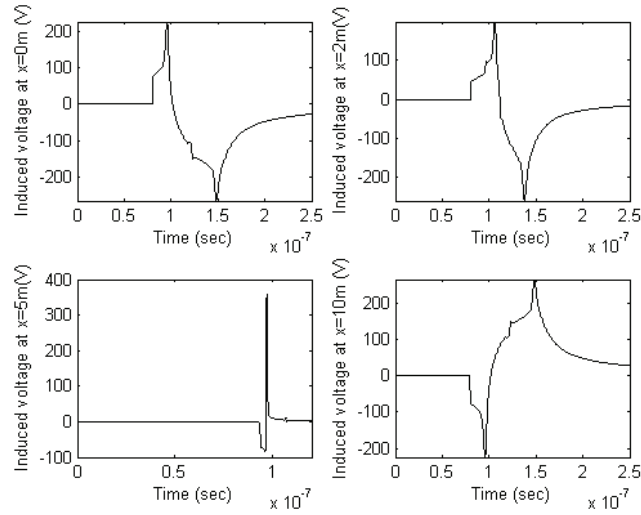


Figure 19. Induced voltage on the shield at different points

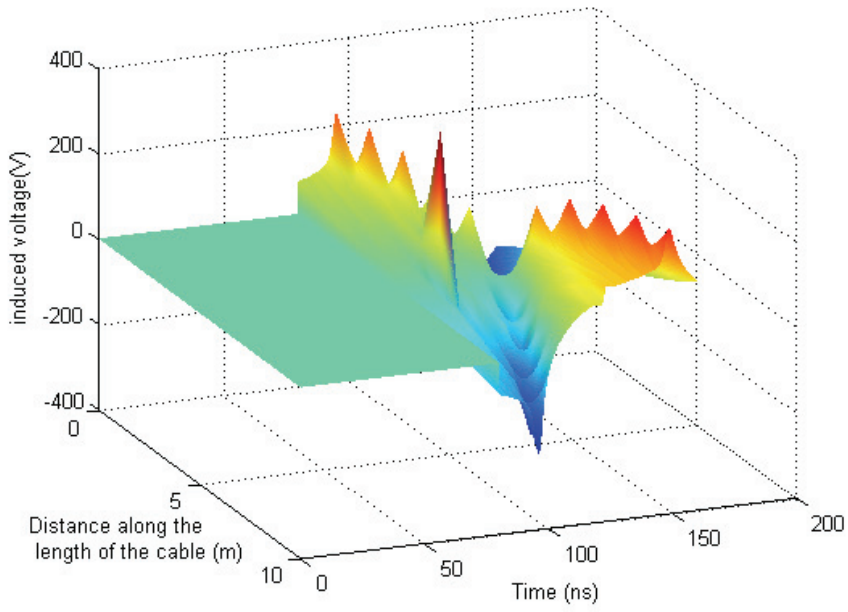


Figure 20. Induced voltage on the shield at different points as a mesh plot

These phenomena are more clearly seen in the figure 20 where a mesh plot of the induced voltage is plotted. Here we can see the gradual shift of the peak voltage to the right from $x=5m$ and beyond and a gradual shift in the peak to the left side for x less than $5m$. The peak shows a gradual reduction with the distance.

On the inner conductor, the induced voltage is obtained as a result of the current induced on the shield and the transfer impedance of the shield. The induced voltage on the conductor is computed at points $0m$, $2m$, $5m$ and $10m$ and is plotted in figure 21. The peak value of the voltage is respectively $23mV$, $12mv$, $-25mv$ and $-23mv$. The induced voltage in the inner conductor is negative of that in the shield at the respective points because the current flows in the opposite direction in the inner conductor as compared to that in the shield. The time of occurrence of the peak decreases from the right end of the cable to the middle and then again increases to the left, at the same time maintaining a similarity between the identical points on either side of the $x=5m$. These details are also seen in the mesh plot shown in figure 22.

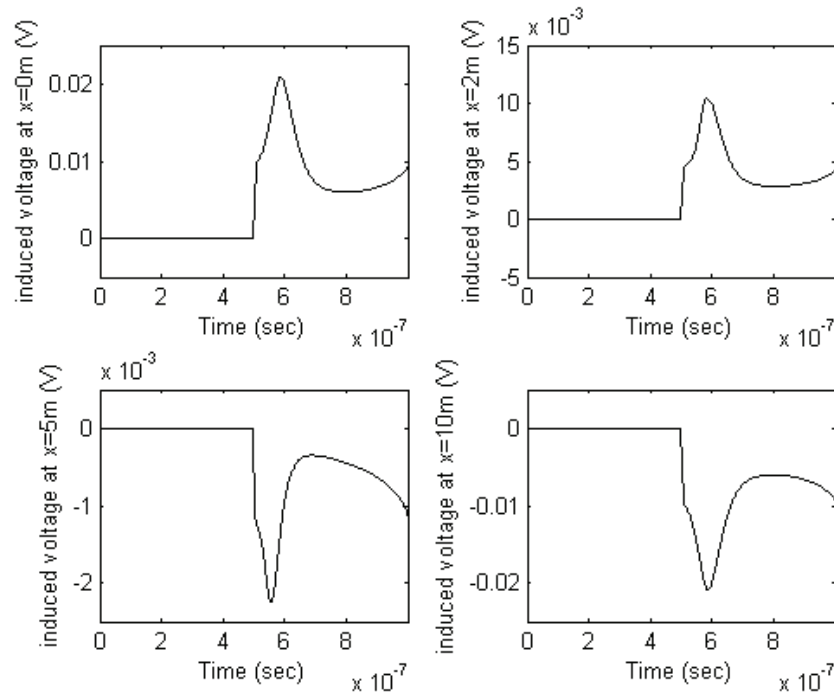


Figure 21. Induced voltage on the inner conductor at different points

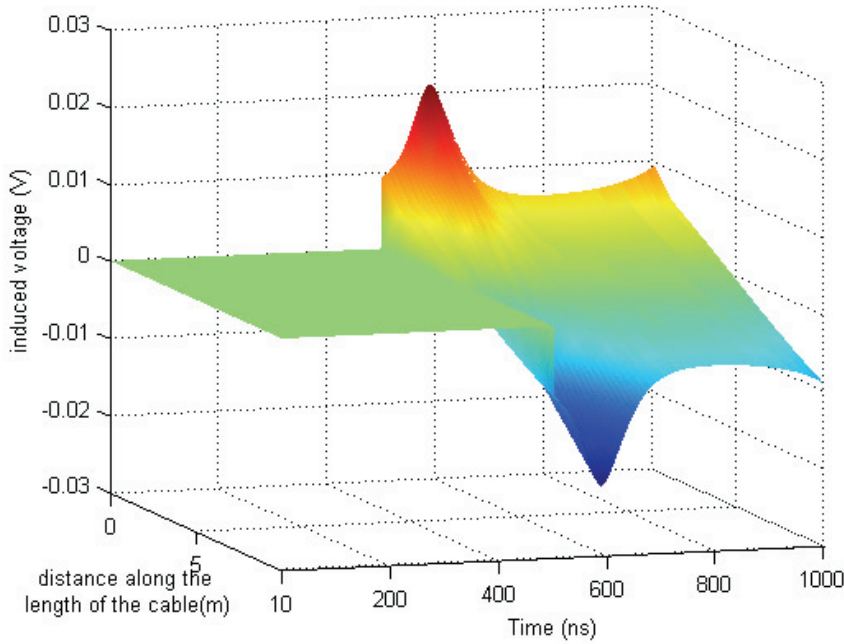


Figure 22 Induced voltage in the inner conductor at different points as a mesh plot

Conclusions:

The IRA antenna is analyzed for the electric fields and is found to have prominent boresight radiation. The width of the boresight radiation depends upon whether the observation point is in the near or in the far field. Using this data as the source, the field along the cable is computed and hence the induced voltage and current is determined. It can be seen that induced current gets reduced by a factor of around 1000 due to the shield properties and also the induced voltage by a factor of 100. But as this is a communication cable even this voltage and current may be large enough to cause a temporary upset of the data in the conductor. Of course, more powerful IRAs will induce even higher induced parameters in the communication cables.

References

1. C. E. Baum and E. G. Farr, "Impulse radiating antennas," in *Ultra-Wideband, Short Pulse Electromagnetics*. H. Bertoni *et al.*, Eds. Plenum, New York, 1993, pp. 139–147.
2. D. V. Giri, **High-Power Electromagnetic Radiators: Nonlethal Weapons and Pother Applications**, Harvard University Press, 2004.
3. D. V. Giri and F. M. Tesche , "Classification of Intentional Electromagnetic Environments", Special Issue on High-Power Electromagnetics (HPEM) and Intentional Electromagnetic Interference (IEMI), *IEEE Transactions on Electromagnetic Compatibility*, Volume 46, Number 3, August 2004, pp 322-328.
4. D. V. Giri, J. M. Lehr, W. D. Prather, C. E. Baum, and R. J. Torres, "Intermediate and far fields of a reflector antenna energized by a hydrogen spark-gap switched pulser", *IEEE Transactions on Plasma Science*, Vol. 28, No. 5, pp.1631-1636, October 2000.
5. C. E. Baum, "Radiation of impulse-like transient fields," Sensor and Simulation Note 321, Nov. 1989.
6. D. V. Giri, H. Lackner, I. D. Smith, D. W. Morton, C. E. Baum, J. R. Marek, W. D. Prather, and D. W. Scholfield, "Design, fabrication, and testing of a paraboloidal reflector antenna and pulser system for impulse-like waveforms," *IEEE Trans. Plasma Sci.*, Vol. 25, No. 2, pp. 318–326, Apr. 1997.
7. Balanis C, *Antenna Theory*, John Wiley and Sons, New York, 1982.
8. E .F. Vance, *Coupling to shielded cables*, Wiley- Interscience, New York, 1978.
9. E. Petrache, M. Paolone, F. Rachidi, C. A. Nucci, V. Rakov , M. Uman, D. Jordan, K.Rambo, J. Jerauld, M. Nyffeler and J.Schoene, "Lightning induced currents in buried coaxial cables: A frequency domain approach and its validation using rocket triggered lightning", *J. Electrostat.*, Vol.65, No.5-6, pp. 322-328, May 2007.
10. E. F. Vance, "Internal Voltages and Currents in Complex Cables", Interaction Note 8, June 1967.
11. F. M. Tesche, M. Ianoz, T. Karlsson, *EMC Analysis Methods and Computational Models*, Wiley - Interscience, New York, 1997.
12. E. D. Sunde, *Earth conduction effects in transmission systems*, Dover, New York, 1968.